IOP Conf. Series: Materials Science and Engineering **438** (2018) 012016 doi:10.1088/1757-899X/438/1/012016

Effects of Gd and Cr co-doping on multiferroic properties of $Bi_{0.9}Gd_{0.1}Fe_{(1-x)}Cr_xO_3$ (x=0–0.08)

M.N. Hossain, M.A. Matin, M.A. Hakim, M.F. Islam

Department of Glass and Ceramic Engineering (GCE), Bangladesh University of Engineering and Technology, Dhaka 1000, Bangladesh

Abstract. Gd and Cr co-doped $Bi_{0.9}Gd_{0.1}Fe_{(1-x)}Cr_xO_3$ (x=0–0.08) nanoparticles were synthesized via sol-gel method. Precursor salts of bismuth, iron, gadolinium and chromium were used as starting raw materials. Obtained nanoparticles were annealed at various temperatures between 400–700 ºC. Optimal properties were found to display at 600 ºC. X-ray diffraction (XRD) patterns revealed that the partial substitution of Bi^{3+} by Gd ions and Fe^{3+} by Cr ions in $BiFeO_3$ (BFO) resulted in evolution of phase transition from rhombohedral to orthorhombic structure. The average crystallite size was found to vary from 16 to 68 nm depending on doping level. The field emission scanning electron micrographs demonstrated a distinct morphology of spherical and nano-sized particles. Ferroelectric measurements showed a substantial improvement in polarization in doped BFO under an applied field of ± 30 kV/cm. Magnetic properties measured at room temperature showed enhanced ferromagnetic characteristics with increasing doping level of Cr up to 6 % (at.) compared to that of un-doped BFO. An asymmetric shift both in the field and magnetization axes of M-H loops was also observed.

1. Introduction

$BiFeO_3$ is one of the most promising multiferroic material which exhibits ferroelectric properties in combination with ferromagnetic properties in the same phase. It is an exciting candidate for contemporary, modern and novel applications due to mutual controllability of the electric polarization with a magnetic field and magnetization by an electric field [1]. $BiFeO_3$ has rhombohedrally distorted perovskite ABO_3 structure. It is ferroelectric below T_C 829.85 ^{0}C and antiferromagnetic below T_N 369.85 ^{0}C. Previous research emphasized that impurity free un-doped $BiFeO_3$ is hard to achieve [3]. Various impurity phases include $Bi_2Fe_4O_9$, $Bi_{36}Fe_{24}O_{57}$ and $Bi_{25}FeO_{40}$ [4]. Magnetic ordering of $BiFeO_3$ is of antiferromagnetic type. It has a spiral modulated spin structure (SMSS) with an incommensurate long wavelength period of 62 nm [6]. This spiral spin structure cancels the macroscopic magnetization and prevents the observation of the linear magnetoelectric effect. However, $BiFeO_3$ suffers from current leakage due to the existence of a large number of charge centers caused by oxygen ion vacancies. These problems restrict the use of $BiFeO_3$ for fabrication of multifunctional devices. To overcome these problems, some attempts have already been undertaken such as enhancing magnetism and ferroelectricity in $BiFeO_3$ by the partial substitution of Bi^{3+} by ions such as Sm^{3+},Nd^{3+} etc., and also substitution of Fe^{3+} by ions such as Cr^{3+}[5] or simultaneous minor substitution of Bi^{3+} and Fe^{3+} by ions such as La^{3+} and Mn^{3+} or La^{3+} and Ti^{4+} respectively [2]. The

partial substitution of Bi^{3+} with ions having higher ionic radii has been found to effectively suppress the spiral spin structure of $BiFeO_3$ giving rise to the appearance of weak ferromagnetism [5]. It was reported that, different kind of doping at A site, specially the single doping of Gd in place of Bi enhances the room temperature magnetization of $BiFeO_3$ as well as improves the phase purity of $BiFeO_3$ [3]. It is also reported that at 200 K due to the substitution of Fe by Cr the area of the magnetization versus magnetic field (M-H) curve increased compared to that of pure $BiFeO_3$ but the M-H loop was still very narrow [5]. Thus, in the present investigation, we studied the effect of co-doping of magnetic Gd and non-magnetic Cr in place of Bi and Fe respectively in $BiFeO_3$. In this context, nominal compositions of $Bi_{0.9}Gd_{0.1}Fe_{(1-x)}Cr_xO_3$ (x=0–0.08) functional multiferroics were synthesized by sol-gel method and their structure, morphology, ferroelectric and magnetic properties were investigated.

2. Experimental

Bismuth nitrate, $Bi(NO_3)_2.5H_2O$ of purity 99% (Merk, India) and iron nitrate, $Fe(NO_3)_3.9H_2O$ of purity 98% (Merk, India) were used to synthesize $BiFeO_3$ by sol-gel method. Stoichiometric proportion of precursors were initially dissolved in deionized water. For Gadolinum (Gd) and Chromium (Cr) co-doped $Bi_{0.9}Gd_{0.1}Fe_{(1-x)}Cr_xO_3$ (x = 0–0.08), gadolinium nitrate, $Gd(NO_3)_3.6H_2O$ of purity 99.99% (Sigma-Aldrich Co., Germany) and chromium nitrate, $Cr(NO_3)_3.9H_2O$ of purity 99% (Sigma-Aldrich Co., Germany) precursors were used in required stoichiometry with BFO chemistry. When the solution was transparent, citric acid ($C_6H_8O_7$) was added to the solution to complex the metal cations. The solution was then stirred and heated at 70 ºC for 3 h to form a transparent blackish-red sol. Next, an appropriate amount of ethylene glycol ($C_2H_6O_2$) was added as a polymerization agent into the solution. Ammonium hydroxide (NH_4OH) was added to maintain pH. The resultant solution was then heated at 85 ºC to initiate the polymerization reaction and a few minutes later a gel was formed with vigorous boiling and fuming. The gel was dried in a drier to obtain xerogel. The xerogel thus obtained was then ground into powders and annealed at 400–700 ºC for 2 h in static air to obtain un-doped BFO and doped BFO nanoparticles. To determine crystallinity and phase(s) of synthesized nanopowders, X-ray diffraction (Empyrean, PANalytical, Netherlands) was employed. Particle morphology was analyzed using field emission scanning electron microscope (JSM 7600F, Japan). Ferroelectric properties were measured using Precision Multiferroic Test System (Radiant Technologies, USA). Magnetic measurements were conducted using a Vibrating Sample Magnetometer (Micro Sense EV9, USA).

3. Results and discussion

Figure 1 shows XRD patterns of the $Bi_{0.9}Gd_{0.1}Fe_{(1-x)}Cr_xO_3$ (x=0–0.08) ceramics sintered at 600 ºC indicating the formation of well-crystalline structure. Rietveld refinement of the nanoparticles was carried out by High Score Plus Software and calculated the particle size and lattice strain are presented in Table 1. There are small traces of secondary phase $Bi_2Fe_4O_9$ as marked by * appeared in the un-doped BFO samples. The apparently unavoidable formation of secondary phases during the sol-gel synthesis of un-doped $BiFeO_3$ based materials have been reported earlier [5]. Suppression of the secondary phase in single phase BFO is a major concern because bismuth and/or iron vacancies help to create these types of impurity phases. Interestingly, in this research, second phases (*) $Bi_2Fe_4O_9$ (Fe rich phase) were almost vanished due to doping of Gd^{3+} in BFO. The decrease in the peak intensities for (x = 0–0.08) indicates the incorporation of Cr in $Bi_{0.9}Gd_{0.1}Fe_{(1-x)}Cr_xO_3$ (x = 0–0.08) ceramics [6]. Furthermore, the twin peaks observed at 2θ= 32º , 52º , and 57º merges to form a broadened peak which becomes weak and tend to dissolve due to Cr doping. Merging of peak at around 2θ = 32º as Cr content increases suggests a structural change from rhombohedral to orthorhombic and is consistent with that reported earlier [7]. We calculated the average crystallite size with the Scherrer equation shown, $D = k\lambda / \beta \cos\theta$, here β is full width at half maximum intensity (FWHM), k is the dimensionless constant with a typical value of 0.9, λ is the wavelength of Cu Kα radiation. The

crystallite size was found to decrease from 68 nm to 16 nm in Gd^{3+} doped BFO. Further addition of doping agent Cr^{3+} in BGFO, the crystallite size increased up to 29 nm for 6% Cr doping.

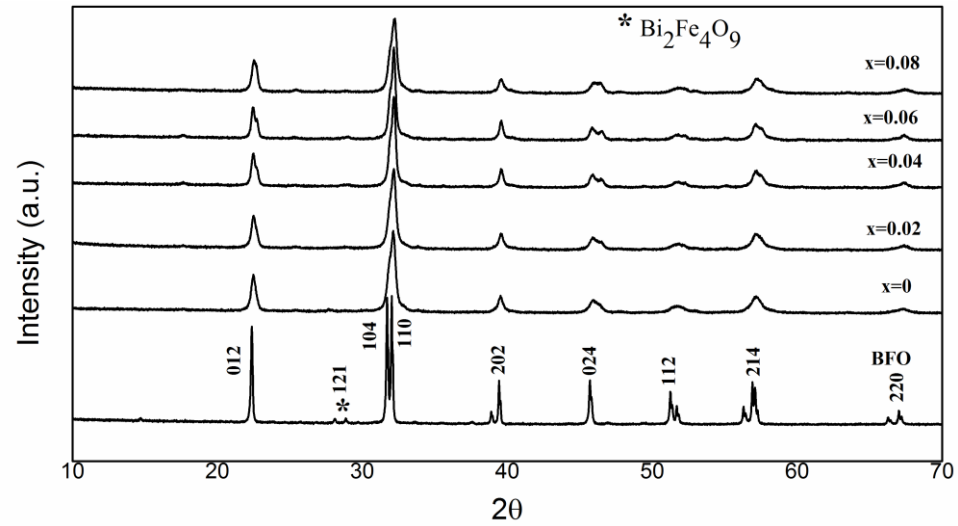

Figure 1: X-ray diffraction patterns of un-doped $BiFeO_3$ and doped $BiFeO_3$ ($Bi_{0.9}Gd_{0.1}Fe_{(1-x)}Cr_xO_3$) nanoparticles annealed at temperature 600 °C.

Lattice strain was also calculated using Bragg's law, $d = n\lambda / 2\sin\theta$, here d is lattice spacing and n is the order of reflection. Lattice strain, $\varepsilon = \Delta d/d_1$ where $\Delta d = d_1 - d_2$. A shift in the peak positions was observed with Gd (and/ Cr) doping. As peaks shift to a higher degree (from right to left) the inter planer spacing reduces as a result the lattice strain increases and may shrink the crystal structure. From Table 1 one can see that the lattice strain increases from 0.186% to 0.772% after Gd doping. More interestingly, lattice strain was found to decrease up to 0.433% due to co-doping of Gd and Cr in BFO.

Table 1. Refined structural parameters, calculated crystallite sizes (d) along with volume and lattice strain values and % of phases of $BiFeO_3$ and $Bi_{0.90}Gd_{0.10}Fe_{1-x}Cr_xO_3$. (x = 0-0.08).

Composition [$Bi_{0.90}Gd_{0.10}Fe_{(1-x)}Cr_xO_3$]	a (Å)	c (Å)	R3c %	$Pn2_1a$ %	d [nm]	ε [-]
BFO	5.57761	13.86779	100	-	68	0.186
x=0	5.55939	13.78815	57.2	42.8	16	0.772
x=0.02	5.57198	13.81291	50.1	49.8	24	0.519
x=0.04	5.56491	13.79472	49.7	50.3	26	0.447
x=0.06	5.56343	13.80535	45.4	54.6	29	0.433
x=0.08	5.56356	13.78329	46.5	53.5	22	0.573

To investigate the morphology of synthesized nanoparticles, secondary electron microscopy was conducted for all samples. Figure 2(a) shows the morphology of un-doped BFO. Grain shape was not spherical and homogeneous. An average grain size of 185 nm was obtained. SEM micrograph of 10% Gd doped $Bi_{0.9}Gd_{0.1}FeO_3$ sample is presented in Figure 2(b).The average grain size was found to be 62 nm. Figure 2(c) shows the microstructure of the 2 % Cr doped $Bi_{0.9}Gd_{0.1}Fe_{(1-x)}Cr_xO_3$. For this sample, the average grain size was measured to be 53 nm. In addition, the grain size distribution was found to be quite homogeneous. The further increase of the Cr content to 4 % (x =0.04) reduced the average grain size to 50 nm (Figure 2(d)) as well as made the distribution of the grains is more uniform. Notably, increase of the Cr content from x =0.04 to x =0.06 and 0.08 (Figures 2 (e) and (f)) the

average grain size becomes 48 nm and 72 nm respectively. Due to the substitution of Cr the average grain size was reduced. Thus, with increasing Cr doping a decreasing trend of the average grain size was observed which is consistent with our findings from XRD results.

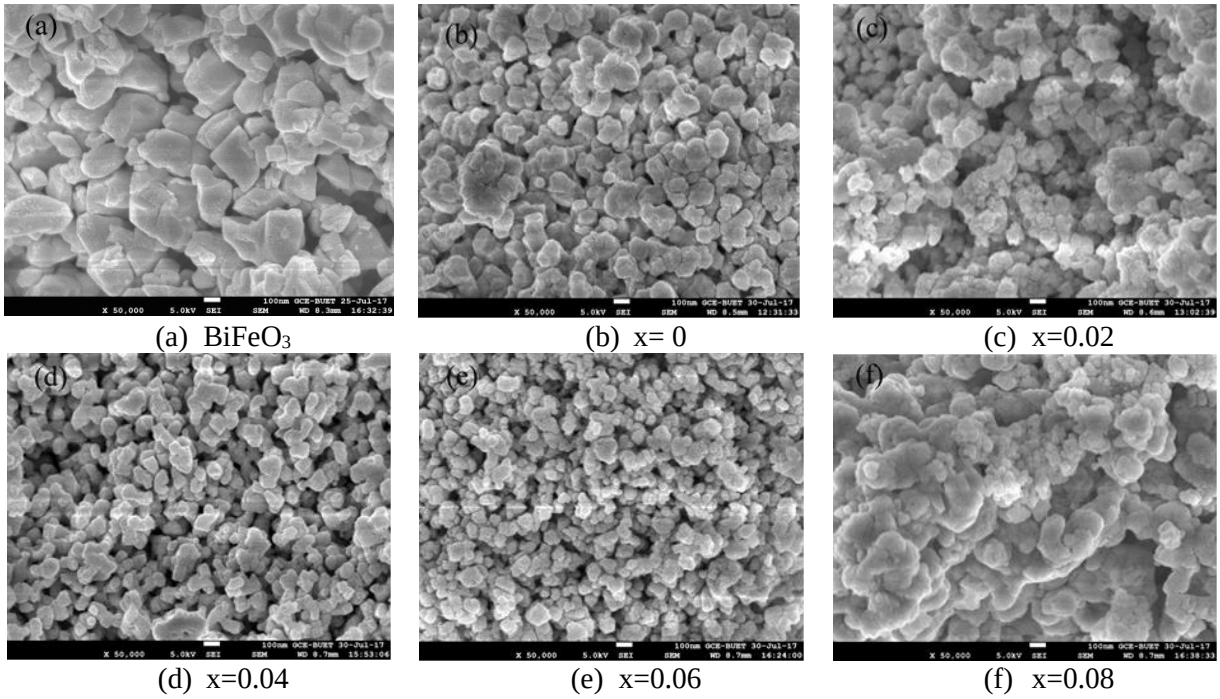

(a) $BiFeO_3$ (b) x= 0 (c) x=0.02

(d) x=0.04 (e) x=0.06 (f) x=0.08

Figure 2. FESEM micrographs of $BiFeO_3$ and $Bi_{0.9}Gd_{0.1}Fe_{(1-x)}Cr_xO_3$ (x = 0-0.08) nanoparticles: (a) $BiFeO_3$, (b) x= 0, (c) x=0.02, (d) x=0.04, (e) x=0.06, (f) x=0.08 annealed at 600 ºC for 2 hr in air.

However, for 8% Cr doping, the average grain size reduced but due to agglomeration effect it measured to be bigger (breaking the normal trend of decreasing). Previous investigation suggested that the grain growth depends upon the concentration of oxygen vacancies and diffusion rate of the ions [7]. Large number of oxygen vacancies generate in pure $BiFeO_3$ due to highly volatile nature of Bi. Therefore, the significant reduction of the average grain size in Gd and Cr co-doped $BiFeO_3$ samples could be interpreted by the suppression of the formation of oxygen vacancies because of the requirements of the charge compensation. The decreased oxygen vacancies may lead to a lower grain growth rate which is actually a consequence of slower oxygen ion motion [8].

Presented in Figure 3 are P-E hysteresis loops of doped BFO captured at room temperature with an applied field of ± 30 kV. The P-E loop of un-doped BFO is also given as an inset for comparison. Such a shape of P-E loop in un-doped BFO resulted from huge leakage current. Encountered oxygen vacancies may be accounted for this [12]. In contrast, the P-E loops of doped-BFO showed much improved saturation resulting comparatively higher remnant polarization. However, with 10% Gd + 2-6% Cr doping, a gradual improvement in ferroelectric properties was observed in synthesized nanoparticles compared to 10% Gd doped one. With 10% Gd^{3+} doping ionic radii difference may bring about further tilting of the structure resulting an overall improvement in ferroelectric properties. However, we speculate that with the addition of Cr^{3+} dopant at B-site (at the centre of oxygen octahedra) the tilting is in opposite direction to that induced by Gd^{3+} doping. Moreover, the exchange interaction between dissimilar magnetic Gd^{3+} and Cr^{3+} ions could play a role.

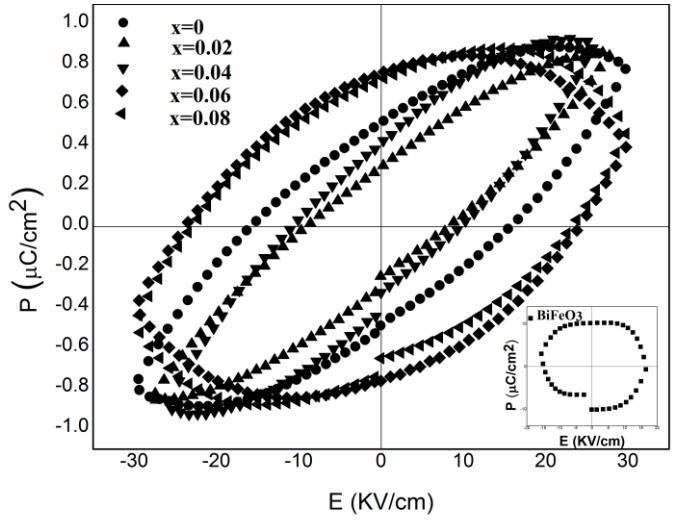

Figure 3. P-E hysteresis loops of $BiFeO_3$ and $Bi_{0.9}Gd_{0.1}Fe_{(1-x)}Cr_xO_3$ nanoparticles at applied field ± 30 kV/cm.

From figure 3, we can see that at low applied field the $Bi_{0.9}Gd_{0.1}Fe_{0.98}Cr_{0.02}O_3$ shows a maximum remanent polarization (P_r = 1.21 μC/cm^2) compared to others (shown in table 2), but the shape of P-E loop is less elliptical. In the case of the $BiFe_{0.90}Gd_{0.10}O_3$ nanoparticles annealed at 600 °C, having the smallest particle size (16 nm), the P-E loop become more and more typical than other compositions which may be due to their reduced leakage current density [9,12].

Table 2. P-E loops and their remanent polarization, coercivity and maximum polarization

Sample $Bi_{0.9}Gd_{0.1}Fe_{(1-x)}Cr_xO_3$	Remanent Polarization, P_r (μC/cm^2)	Coercivity (KV/cm)	P_{max} (μC/cm^2)	Saturation Polarization (KV/cm)	d [nm]
BFO	-	-	-	30	68
x=0	0.16	0.69	0.25	30	16
x=0.02	1.21	0.36	3.49	28	24
x=0.04	0.15	0.63	0.33	26	26
x=0.06	0.41	1.64	0.22	30	29
x=0.08	0.73	1.27	0.48	30	22

Figure 4 shows M-H hysteresis curves for un-doped $BiFeO_3$, and (Gd and Cr) co-doped $Bi_{0.9}Gd_{0.1}Fe_{(1-x)}Cr_xO_3$ (x = 0–0.08) ceramics measured at RT with an applied magnetic field of up to ± 20 kOe. All the samples show unsaturated magnetization loops which confirm the basic antiferromagnetic nature of the samples. The un-doped $BiFeO_3$ sample possesses a very narrow hysteresis loop with a very small but non zero remanent magnetization (0.001 emu/g) and a coercive field of 62 Oe at RT. This is due to the fact that pure $BiFeO_3$ is antiferromagnetic (AFM) which does not possess any spontaneous magnetization but has a residual magnetic moment for a canted spin structure.

From Figure 5, a nonzero remanent magnetization and coercive field are observed. The remanent magnetization (M_r) is defined as $Mr = |M_{r1}-M_{r2}|/2$ where M_{r1} and M_{r2} are the magnetization with positive and negative points of intersection with H = 0 respectively [2]. The coercive field (H_c) is given as $H_c = |H_{c1} - H_{c2}|/2$, where H_{c1} and H_{c2} are the left and right coercive fields respectively [9].

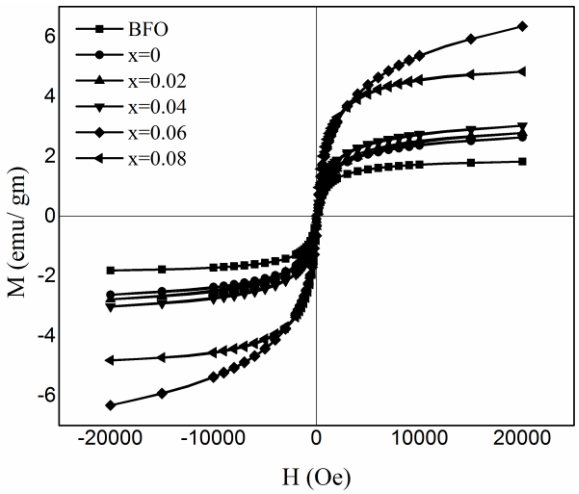

Figure 4. M-H hysteresis curves of $BiFeO_3$ and $Bi_{0.9}Gd_{0.1}Fe_{(1-x)}Cr_xO_3$ (x = 0-0.08) nanoparticles measured at RT.

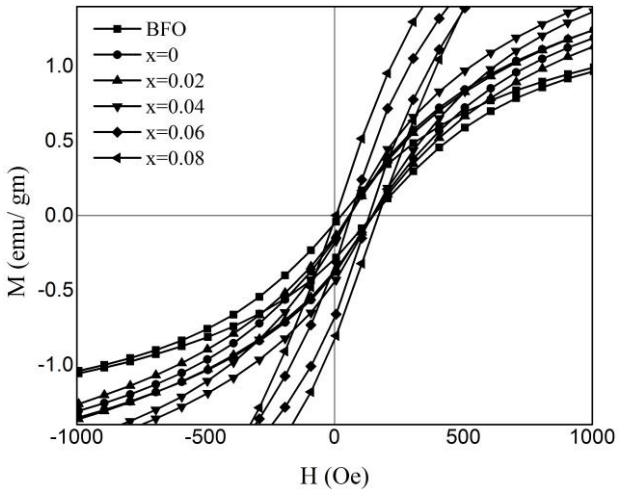

Figure 5. An enlarged view of the low-field M-H hysteresis loops of $Bi_{0.9}Gd_{0.1}Fe_{(1-x)}Cr_xO_3$ (x = 0-0.08) samples obtained at RT.

Calculated values of M_r and H_c are presented in Table 3. An increment of the 2% Cr doping concentration in place of Fe in $Bi_{0.9}Gd_{0.1}Fe_{(1-x)}Cr_xO_3$ (x=0–0.08) increased the saturation magnetization although the coercivity decreased. A further increase in Cr doping concentration to 8% dramatically enhanced M_r and H_c. Due to 10% Gd doping in $BiFeO_3$ improved magnetic property was observed as reported earlier [7]. This enhancement of the magnetization at RT was attributed to the structural distortion in the perovskite with change in Fe–O–Fe angle. It was expected that this structural distortion could lead to suppression of the spin spiral and hence enhanced the magnetization in synthesized multiferroic system.

Table 3. M-H loops and their remanant magnetization, coercivity, saturation magnetization of $BiFe_{1-x}Cr_xO_3$ (x = 0–0.08) ceramics at RT

Sample $Bi_{0.9}Gd_{0.1}Fe_{(1-x)}Cr_xO_3$	Remanant magnetization, M_r (emu/g)	Coercivity H_c (Oe)	Saturation magnetization M_s (emu/g)	d [nm]
BFO	0.11	62	1.9	68
x=0	0.28	45	2.9	16
x=0.02	0.13	48	3.1	24
x=0.04	0.16	46	3.5	26
x=0.06	0.12	36	7.1	29
x=0.08	0.42	83	5.0	22

Similar to 10% Gd doped $Bi_{0.9}Gd_{0.1}FeO_3$, the hysteresis loops of Gd and Cr co-doped ceramics were not really saturated at 20 kOe. However, a significant enhancement in remanent magnetization and coercive field was observed with the increase in Cr doping concentration in $Bi_{0.9}Gd_{0.1}Fe_{(1-x)}Cr_xO_3$ (x = 0–0.08) multiferroics. In an investigation, room temperature magnetic properties were carried out for only Cr doped $BiFe_{1-x}Cr_xO_3$ ceramics with varying x up to 0.08 [5]. In that investigation, the highest saturation magnetization of 0.75 emu/g was reported for 6% Cr doped (not co-doped). In the case of presently investigated Gd and Cr co-doped ceramics $Bi_{0.9}Gd_{0.1}Fe_{0.94}Cr_{0.06}O_3$, the saturation magnetization is 7 emu/g, which is nine times higher. The coercive field is also lower for Gd and Cr co-doped samples compared to that of only Cr doped $BiFe_{1-x}Cr_xO_3$ (x = 0–0.08) ceramics. Hence, it is

clear that Gd and Cr co-doped $Bi_{0.9}Gd_{0.1}Fe_{(1-x)}Cr_xO_3$ ceramics exhibit enhanced magnetic properties at RT showing weak ferromagnetic (WFM) antiferromagnetism.

The statistical distribution of Fe^{3+} and Fe^{2+} (created due to charge compensation) ions in the octahedral also lead to an increase in magnetization and weak ferromagnetism. However, for 8% Cr doping in $Bi_{0.9}Gd_{0.1}Fe_{(1-x)}Cr_xO_3$, the remanent magnetization and coercive field both again decreased and the antiferromagnetic order typical to $BiFeO_3$ parent phase is likely to be recovered. This might be associated with the structure phase transition from rhombohedral to orthorhombic at x = 0.08.

However, beside the enhanced room temperature magnetic properties in Gd and Cr co-doped $Bi_{0.9}Gd_{0.1}Fe_{(1-x)}Cr_xO_3$ (x = 0–0.08) ceramics, the most intriguing feature observed from the enlarged view (Figure 5) of the low field M-H hysteresis loops is their asymmetric behavior. An asymmetry exhibiting shifts both in the field and magnetization axes can clearly be observed for all the samples. This indicates the presence of exchange bias (EB) effect in it. The presence of EB phenomenon in these multiferroics was assumed to be associated with induced exchange anisotropy at the interface between FM and AFM phases.

4. Conclusions

Un-doped BFO and doped $Bi_{0.9}Gd_{0.1}Fe_{(1-x)}Cr_xO_3$ functional multiferroics were successfully synthesized using sol-gel method. XRD patterns shows the coexistence of both the Rhombohedral phase and the Orthorombic phase in the ceramic. The crystallite size (obtained from Rietveld analysis) reduced significantly from 68 nm to 16 nm due to increasing Cr doping level. However, the measured particle size in SEM was found to be substantially higher due mainly to agglomeration effects observed in synthesized nanoparticles (with high surface energy). The ferroelectric property namely remanent polarization and coercivity was enhanced due to co-doping. Due to the combined effects of Gd and Cr, magnetic properties of these ceramics were improved at RT. However, M-H hysteresis loops of co-doped BFO nanaoparticles demonstrate an asymmetric shift towards the field axis. The remanent magnetizations and saturation magnetizations were improved at room temperature but coercivity decreased.

Acknowledgments

This research is supported by the Department of Glass and Ceramic Engineering, Bangladesh University of Engineering and Technology (BUET), Dhaka, Bangladesh.

5. Reference

[1] W. Eerenstein, N. D. Mathur, and J. F. Scott, Nature 442, 759 (2006).
[2] G. Anjum, R. Kumar, S. Mollah, D. K. Shukla, and C. G. Lee, J. App. Phys.107, 103916 (2010).
[3] Q. H. Jiang, C. W. Nan, and Z. J. Shen, J. Am. Ceram. Soc. 89, 2123 (2006).
[4] T. Munoz, J. P. Rivera, A. Monnier, and H. Schmid, Jpn. J. Appl. Phys., Part 1 24, 1051 (1985).
[5] Amit Kumar, K.L. Yadav, Materials Science and Engineering B 176, 227–230 (2011).
[6] R. A. Agarwal, S. S. Ashima, and N. Ahlawat, J. Phys. D: Appl. Phys. 45, 165001 (2012).
[7] M. A. Basith, O. Kurni, M. S. Alam, B. L. Sinha, and B. Ahmmad, Journal of Applied Physics. 115, 024102 (2014).
[8] Z. Chaodan, Y. Jun, Z. Duanming, Y. Bin and Z. Wenli, Integr. Ferroelectr. 94, 31 (2007).
[9] Y. Guo, L. Shi, S. Zhou, W. Liu, and S. Wei, J. Phys. D: Appl. Phys. 46, 175302 (2013).
[10] S. W. Cheong and M. Mostovoy, Nature Mater. 6, 13 (2007).
[11] P. Tirupathi and A. Chandra, J. Alloys Compd. 564, 151 (2013).
[12] A. Ianculescu, F. Prihor, P. Postolache, N. Drgan, and D. Crian, Ferroelectrics 391, 67 (2009).
[13] Chang, C., Mao, D., Int. J. Chem. K., 39, 75, 2007.
[14] R. Ramesh, Nature 461, 1218 (2009).